Available online at www.sciencedirect.com
ScienceDirect
International Journal of Mass Spectrometry 268 (2007) 122–130
International Journal of Mass Spectrometry
www.elsevier.com/locate/ijms

Positive and negative analyte ion yield in matrix-assisted laser desorption/ionization

Maxim Dashtiev [a,b], Esther Wäfler [a], Ulrich Röhling [c], Michael Gorshkov [b], Franz Hillenkamp [c], Renato Zenobi [a,*]

[a] *Department of Chemistry and Applied Biosciences, ETH Zürich, CH-8093 Zürich, Switzerland*
[b] *Institute for Energy Problems of Chemical Physics, Russian Academy of Sciences, Moscow, Russia*
[c] *Institute of Medical Physics and Biophysics, University of Münster, Münster, Germany*

Received 26 February 2007; received in revised form 27 June 2007; accepted 3 July 2007
Available online 10 July 2007

Abstract

The ratios of positive to negative analyte ion yields for matrix-assisted laser desorption ionization were studied for fibrinopeptide A, angiotensin I and bradykinin in combination with six matrices (CHCA, DHB, 4-NA, ATT, ANP, 5-AQ). The selection of these particular compounds was based on their acid/base properties. The measurements were carried out on two different time-of-flight instruments, one of which was equipped with a charge collection detector. The findings are: (i) for a desorption from a non-metallic substrate the total positive/negative ion yield ratio is ≈1. (ii) The analyte positive/negative ion yield is strongly dependent on many factors, and generally scatters a lot. More acidic matrices were found to produce a positive/negative analyte ion yield ratio >1, whereas for basic matrices, the ratio was ≤1. (iii) For selected matrices, the positive/negative analyte ion yield ratio follows the acid/base properties of the analyte. (iv) Clear indications for a significant contribution of clusters as carriers of the total charge in MALDI were obtained from the data.

Keywords: MALDI; Ion yield; Ionization mechanism

1. Introduction

Matrix-assisted laser desorption ionization (MALDI) has rapidly become a powerful technique for the analysis of peptides and proteins [1–3]. Mostly, MALDI MS analysis is carried out in positive ion mode [4], although there is no clear evidence that positive ions are always more abundant. In some cases, e.g., the analysis of phosphopeptides or nucleic acids, both in positive and negative modes can be beneficial [5]. Investigation of ion yields in MALDI, and comparison of positive to negative ion yields, can thus be important for practical purposes. The relative yield of positive to negative analyte ions and its dependence on the physical–chemical properties of analyte and matrix as well as the sample preparation conditions is an experimentally accessible parameter, which should allow insights into the ion formation process(es) in MALDI. Surprisingly, very few studies have been published addressing this parameter. The production of positive and negative ions of biomolecules by MALDI was recently studied by simultaneously measuring both polarities in a dual-polarity time-of-flight mass spectrometer [6]. The ion optics were arranged to be able to extract positive and negative ions synchronously with equal efficiency to each corresponding mass analyzer. The spectral patterns obtained in this work for larger peptides/proteins (insulin B-chain and myoglobin) and trihydroxyacetophenone as well as CHCA as matrices were approximately mirror images with opposite polarities, suggesting a comparable yield of positive and negative analyte ions. For angiotensin I a larger positive ion yield was reported. Another example is the analysis of ultrafine particles by direct laser desorption/ionization (no matrix) in a bipolar TOF instrument [7]. More positive than negative ions were observed in this study. As an explanation, the authors suggested that under laser irradiation, ultrafine aerosol particles yield primarily positive ions, neutrals, and electrons. Because of

* Corresponding author. Tel.: +41 44 632 43 76; fax: +41 1 632 1292.
E-mail address: zenobi@org.chem.ethz.ch (R. Zenobi).

1387-3806/$ – see front matter © 2007 Elsevier B.V. All rights reserved.
doi:10.1016/j.ijms.2007.07.001

the small particle size, the density of the plume is low and the probability of electron capture by neutrals and positive–negative charge recombination in the plume are low. This could lead to a positive ion yield greater than the yield of negative ions.

The overall yield of charged species in MALDI is rather low, typically on the order of 10^{-4} [8,9]. In negative mode, in addition to matrix and analyte signals, a signal for electrons has been detected with a FT-ICR instrument for samples prepared on metal substrates [10,11]. From these studies it is clear that photoelectron emission from metal substrates could possibly skew the relative positive/negative ion yield and should be avoided when conducting these experiments.

A number of different ionization mechanisms have been proposed for MALDI [12–17] but none of them explicitly compares the total yields of positive to negative ions nor provides any quantitative predictions. One of the earliest and still often assumed models for MALDI ion formation is a primary photoionization of matrix molecules, followed by a gas-phase proton transfer to analyte ions in the expanding MALDI plume [15,16,18], This process depends critically on the gas-phase basicities of the respective analyte and matrix species, as detailed in the theory section below. We, therefore, decided to systematically measure and compare the yield of positive and negative ions for a several analyte/matrix combinations, three peptides (bradykinin, angiotensin I, fibrinopeptide A), and six matrices (α-cyano-4-hydroxycinnamic acid, CHCA; 2,5-dihydroxybenzoic acid; DHB; 2-amino-5-nitro-4-picoline, ANP; 6-aza-2-thiothymine, ATT; 4-nitroaniline, 4-NA; 5-aminoquinoline, 5-AQ). The selection of these particular compounds is based on their acid/base properties. DHB and CHCA are strongly acidic, ATT and 4-NA are neutral, and ANP and 5-AQ are basic. Fibrinopeptide A is very acidic (sequence ADSGEGDFLAEGGGVR, $M_W = 1536$ Da, calculated p$I = 3.92$,), angiotensin I contains a balanced number of acidic and basic amino acids, leading to a pI close to 7 (sequence DRVYIHPFHL, $M_W = 1296$ Da, calculated p$I = 6.92$), and bradykinin is basic (sequence RPPGFSPFR, $M_W = 1059$ Da, calculated p$I = 12$). Ion yields were measured by time-of-flight mass spectrometry and compared for each combination of peptide/matrix on nonmetallic MALDI targets. In this context, one has to clearly distinguish between *total* ion yield (including matrix signals and chemical noise) which in the absence of electrons should be equal for positive and negative ions, and *analyte* ion yield, which, at least to some extent, is expected to depend on protonation and deprotonation reactions, governed by the acidity/basicity of sample and matrix.

The purpose of this study was to test the hypothesis of whether the gas-phase proton transfer is the dominating process in the formation of analyte ions in MALDI, and whether the predicted dependence on the physical-chemical properties of the matrices and analytes is experimentally observed. In order to achieve this goal, all accessible parameters particularly in the sample preparation, matrix/analyte molar ratio, and irradiation fluence were kept as constant as possible, even if the parameters chosen were not necessarily optimal for a given ion polarity and all analyte/matrix combination.

2. Experimental

2.1. Materials

Bradykinin, angiotensin I, and fibrinopeptide A (human) were purchased from Bachem AG (Switzerland), CHCA (purity 99%) from Sigma (Switzerland), DHB (purity 99%), ANP (purity 98%) from Acros Organics (Switzerland), ATT (purity 99%), 4-NA (purity 99%) and cesium iodide (CsI, purity 99%) from Fluka (Buchs, Switzerland), and 5-AQ (purity 97%) from Aldrich (Buchs, Switzerland). All compounds were used without further treatment or purification.

2.2. Sample preparation

CHCA (10 mg/ml) was dissolved in acetonitrile (ACN) and 0.1% aqueous TFA at a ratio of 70/30. DHB was dissolved in ethanol/H_2O (1:1) at 10 mg/ml. ATT, 4-NA, 5-AQ, and ANP were dissolved in ACN/H_2O (1:1), ATT, 4-NA, and 5-AQ at 10 mg/ml and ANP at 5 mg/ml. All three peptides were dissolved in H_2O to a concentration of 10^{-4} mol/l. Matrix and peptide solutions were mixed at a ratio of ca. 3:2 (3:1 for ANP) to obtain a final molar analyte-to-matrix ratio of 10^{-3}. This ratio was the smallest one which yielded positive as well as negative ion signals for all tested analyte/matrix combinations. All samples were prepared by the standard dried droplet method, depositing 2 μl of sample onto 2 mm × 2 mm pieces of (the insulating) Scotch 810 Magic adhesive tape on the standard Bruker or Shimadzu sample plates. Although certainly not standard practise in most MALDI applications, this precaution was taken to be absolutely certain that skewing of the negative/positive ion yields by electrons emitted from the target can be excluded. For a few selected combinations of analyte and matrix samples prepared on Scotch 810 Magic adhesive tape and on a standard metal sample plate were tested; no significant differences in the spectra were found. Due to their volatility, preparations with 4-NA and 5-AQ for the charge detector measurements involved three subsequent applications of 2 μl each, deposited on top of each other with drying in between, to increase the time available for analysis.

2.3. Mass spectrometry

At ETH Zürich, MALDI-TOF mass spectra were acquired on an AXIMA CFR instrument (Kratos Analytical, Shimadzu Biotech, Manchester, UK) with a drift tube length of 1.2 m. The charge detector spectra were acquired at the University of Münster on a Reflex III instrument (Bruker, Bremen) with a 1.8 m effective flight tube length. Both instruments operate with a nitrogen laser ($\lambda = 337$ nm, 3 ns pulse width, ±3% shot-to-shot energy reproducibility).

Spectra recorded on the AXIMA were collected in reflectron mode with and without delayed extraction. When used, the extraction delay was 200 ns. The accelerating voltage was set to ±20 kV depending on the polarity used. Detector bias was −2 kV. During acquisition the sample target was monitored by a monochrome video-image system (25× magnification). Spec-

tra were the sum of 200 profiles automatically acquired while rastering the selected sample areas.

Spectra on the Reflex III were recorded in linear mode with the "short" setting for the delay chosen, optimial for the peptide mass range. The reproducibility of the laser energy output from shot to shot was 3% SD. This instrument is not set up for spectrum acquisition by scanning selected areas. Sum spectra of 20–50 laser exposures (depending on the matrix) were, therefore, recorded from randomly selected sample spots. For every given sample the threshold fluence for the detection of positive and negative ions was determined with a secondary electron multiplier (SEM) tube detector that could be slid into a position in front of the charge detector. The charge detector spectra of both polarities were then obtained with equal laser fluences at most 30% above the SEM threshold. The floating detector is prone to picking up noise from nearby sources. The limit of detection is, therefore, given by this noise pick-up, in this case mostly from the turbomolecular pumps (see, for example, Fig. 5), rather than the electronic noise of the detector and amplifiers.

All experiments were performed both in negative and in positive modes on identical samples and identical (except for the polarity) instrument settings. To determine the error bars of the data one standard deviation from the mean was calculated. The integration of the spectra from the AXIMA instrument was performed using commercial software (Igor Pro V4.08, Wavemetrics, Lake Oswego/OR).

2.4. Detection

We first performed an experiment with (matrix-free) desorption ionization from CsI crystals. In this experiment, the laser pulse breaks up the solid, which leads to equal number of positively and negatively charged particles (molecular and atomic ions, clusters, chunks of material). Fig. 1 shows positive/negative mode TOF mass spectra of CsI ions and their integrals, which correspond to the total ion currents. With the exception of polarity, both spectra were recorded under identical, typical experimental conditions. Impurities in the negative mode mass spectrum of CsI are from the scotch tape. As can be seen from the Fig. 1 the total positive ion signal is higher than the negative by factor of about 4. The calculated ratio of the total ion currents obtained from five repeat measurements was found to be 3.5 ± 1.2. A comparative experiment with CsI was performed on our home-built internal MALDI source Fourier transform ion cyclotron resonance (FT-ICR) mass spectrometer because (i) no ion guides/optics are used to transmit charged particles and (ii) in ICR, the detection efficiency does not depend on the polarity of the ions. Integration of the mass spectra acquired in the FT-ICR using an insulating sample target gave equal response for both positive and negative modes (data not shown). Repetition of measurements up to five times did not show any difference in the total ion yield in positive and negative modes. Thus, it is obvious that there is a detection discrimination in the AXIMA TOF mass spectrometer. So far, we do not fully understand the reasons for this discrimination. It may be caused by the detector bias potential, which results in post-acceleration favoring detection of positive ions. On our instrument, the detector is

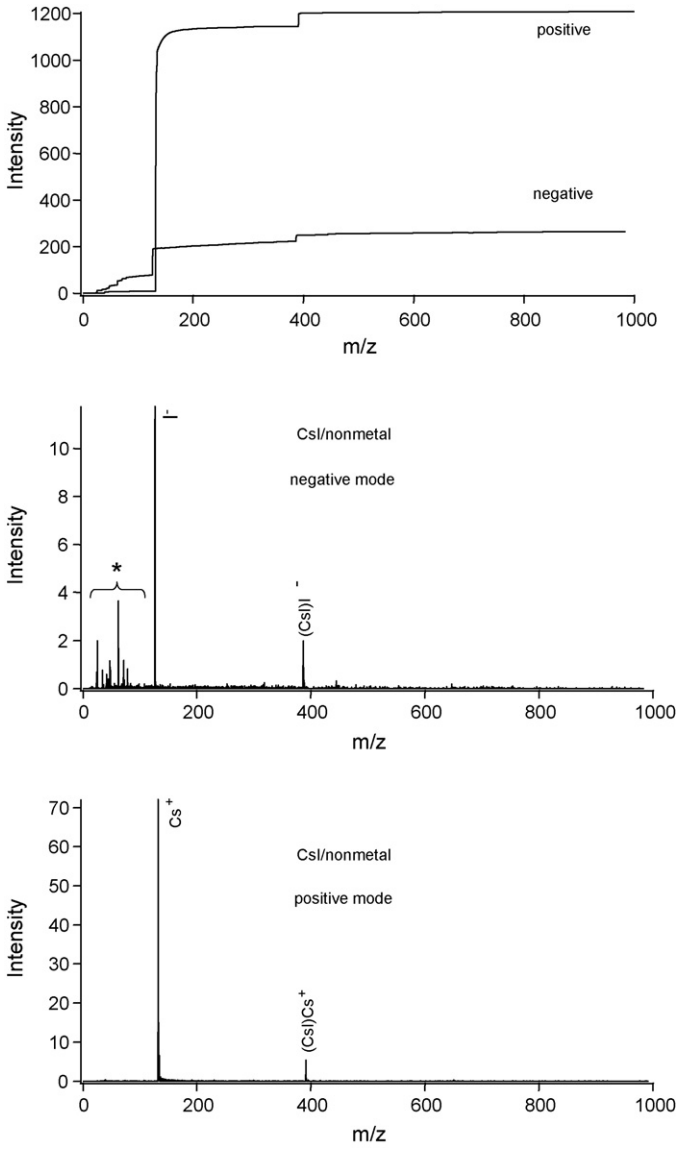

Fig. 1. Laser desorption ionization TOF mass spectra of CsI crystals deposited on a nonconductive substrate, acquired in both positive (bottom) and negative (middle) modes. The integration of the spectra (top) corresponds to the total ion yield. The asterisk indicates impurities.

operated at −2 kV, thus positive ions experience a total acceleration voltage by 22 kV, while negative ions "feel" only 18kV (using ±20 kV extraction). Also, the system configuration (i.e., ion guides, lenses, etc.) may have been optimized for positive ions. We assume that this scaling factor is instrument specific and cannot be directly applied to other mass spectrometers. However, it is important to note that in order to directly compare between experiments on an absolute scale one must take into account this scaling factor. Thus, a factor of 3.5, determined for our particular TOF instrument, was applied when evaluating the data (Table 1, Fig. 6), but neither to raw TOF spectra nor to the integrated spectra shown in the Figs. 3 and 4.

As a second alternative to prevent bias in detecting ions of one polarity over the other, a modified charge detector of the Faraday-cup type was used for the measurements on the Bruker

Table 1
Ratio of positive to negative ion signals for different analyte to matrix combinations measured on the Bruker instrument with the charge detector

Matrix	Analyte					
	Bradykinin		Angiotensin		Fibrinopeptide A	
	Positive/negative analyte ion signal	Positive/negative total ion current	Positive/negative analyte ion signal	Positive/negative total ion current	Positive/negative analyte ion signal	Positive/negative total ion current
CHCA	2.38 ± 1.21 *1.5 ± 0.8*	0.14 ± 0.072 *1.3 ± 0.6*	3.24 ± 2.45	0.36 ± 0.25	1.18 ± 1.10 *0.6 ± 0.3*	0.58 ± 0.59 *0.6 ± 0.3*
DHB	3.78 ± 2.58 *2 ± 1*	0.53 ± 0.26 *1.4 ± 0.6*	2.42 ± 1.61	0.36 ± 0.17	1.04 ± 0.55 *0.6 ± 0.3*	0.48 ± 0.23 *0.6 ± 0.3*
ATT	12 ± 8.7 *0.6 ± 0.4*[a]	0.84 ± 0.48 *0.7 ± 0.4*	2.0 ± 0.96	0.17 ± 0.14	1.19 ± 0.91 *1 ± 0.6*	0.22 ± 0.17 *1 ± 0.5*
4-NA	2.64 ± 1.76 *1 ± 0.6*	0.98 ± 0.44 *1 ± 0.5*	1.12 ± 0.67	0.88 ± 0.62	1.27 ± 0.94 *0.8 ± 0.6*	1.46 ± 1.32 *0.8 ± 0.5*
ANP	1.56 ± 0.73 *3.7 ± 2*[a]	0.80 ± 0.65 *2.5 ± 1*	1.31 ± 0.51	0.63 ± 0.43	0.92 ± 0.78 *0.5 ± 0.2*	0.38 ± 0.40 *0.5 ± 0.2*
5-AQ	0.41 ± 0.54[b]	0.10 ± 0.082	0.89 ± 0.70	0.50 ± 0.64	0.79 ± 0.58	1.17 ± 1.10

Numbers in italics are measurements from the Shimadzu instrument, corrected by a factor of 3.5 to account for the bias for positive ions of this instrument.
[a] These numbers are lower bounds, because signals of negative ions, clearly discernable from matrix signals and noise were obtained only from a very limited number of selected sample spots.
[b] This SD clearly reflects a non-Gaussian distribution of the values.

Reflex III instrument (Fig. 2). The detector and its basic performance has been described in a former publication [19]. In brief, ions are collected by a planar metal plate (1) of 18 mm diameter upon exiting the linear flight tube of the Bruker Reflex III mass spectrometer. Ions entering the space between a fine mesh 300 μm in front of the collector plate induce a charge on the collector plate, which is recorded by a field effect (FET) transistor of 1 GΩ and ca. 12 pF input impedance, followed by an impedance converter amplifier. As discussed in the original publication, the recorded signal reflects the incoming charge as well as any outgoing charge of sputtered secondary ions and electrons. In order to minimize these secondary effects the primary ions were retarded to an impact energy of ca. 700 V before hitting the collector plate held at ±9.3 kV. To this end the whole detector flange was isolated from the drift tube of the mass spectrometer by a 10 cm wide insulating PEEK spacer. In order to keep the offset voltage manageable the spectrometer was tuned down to a ±10 kV ion acceleration instead of the usual ±20 kV. Equipotential lines and selected ion trajectories are also shown in Fig. 2. A graphite tube (2) (for minimal secondary ion generation) of 50 mm i.d. protrudes 50 mm outward from the detector housing into the flight tube. It is held at a potential of ±8.85 kV to focus the incoming ions onto the collector plate. The mesh directly in front of the collector plate (not shown in Fig. 2) was held at a potential of −15 V relative to the plate to prevent residual electrons (and negative ions) from leaving the plate. A second mesh (3) ca. 5 mm in front of the collector at a potential of ±8.6 kV prevents secondary charges, generated by ion impact on the tube or other structures from reaching the collector plate. All of these precautions cannot, however, prevent neutral molecules and clusters, generated by post source decay, from reaching the detector. They impact with the full velocity of their precursor ions and an impact energy which makes sputtering of secondary particles probable. These neutrals will arrive at the detector prior to the ions of equal mass. For the given geometry and potentials they appear at a mass of 0.85 m_{ion} and are clearly visible in the spectra for specific matrix or analyte ions. Their corresponding ions will reach the detector only if their mass is ≥0.93 m_{parent} and with a slight delay relative to the parent ions. The −15 V potential of the mesh in front of the collector plate will allow only positive secondary ions to be extracted. As a result these signals of neutrals will result in a negative step in positive ions spectra and a positive step in the negative ions spectra if the non-decayed ions produce a positive step in both polarities. The signal of the charge detector is coupled to the transient digitizer of the mass spectrometer via an ac-coupling unit with a time constant of several hundred microseconds.

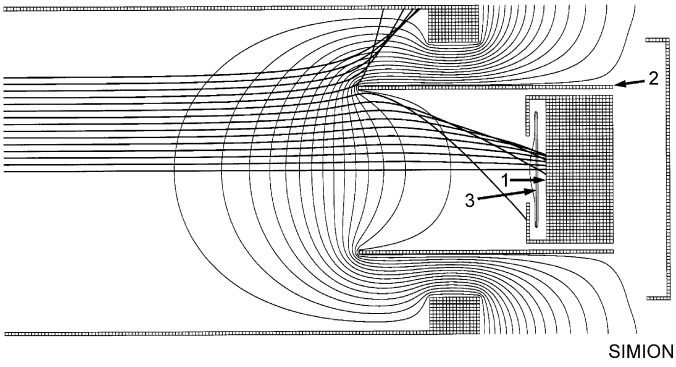

Fig. 2. Geometry of the charge detector with field lines and selected ion trajectories. (1) Charge collector plate at $U_c = \pm 9300$ V. (2) Graphite focusing tube at $U_t = \pm 8850$ V. (3) Second grid at $U_g = 8600$ V. Not shown is a first mesh 300 μm in front of the charge collector plate. The flight tube is at ground potential.

3. Theory

Gas-phase proton transfer can be described using some simplifying assumptions. As a first approximation, protonated analyte ions can be assumed to be produced by the reaction: $A + (M+H)^+ \leftrightarrows (A+H)^+ + M$ (A = analyte, M = matrix), and, likewise, deprotonated analyte by reaction with deprotonated matrix, $A + (M-H)^- \leftrightarrows (A-H)^- + M$. Here, $(M-H)^-$ and $(A-H)^-$ refer to deprotonated matrix and analyte, respectively. The free energies of these equilibriums are given by the differences of the gas-phase basicities of matrix and analyte (deprotonated analyte and deprotonated matrix, respectively, in negative mode), at least in a dense plume without external electric field during extraction delay, where a sufficient number of collisions can occur. If we now express the equilibrium constants for the above protonation/deprotonation reactions with the Gibbs function, $K_{eq} = \exp(-\Delta G/RT)$, we can obtain an expression for the relative concentration of protonated and deprotonated analyte in our "reaction vessel", i.e., the plume:

$$\frac{[A + H^+]}{[A - H^-]} \propto \exp\left\{-\frac{[(GB(M) + GB(M - H^-)]}{RT}\right\} \quad (1)$$

This expression is based on several assumptions: (i) an equilibrium is assumed to be established; (ii) a temperature is assumed to be defined (and known); (iii) the proportionality factor contains the relative concentration of protonated and deprotonated matrix ions, which is assumed to be constant, times a term containing the gas-phase basicities of analyte and deprotonated analyte, $[M+H^+]/[M-H^-] \times \exp\{-[(GB(A) + GB(A-H^-)]/RT\}$.

The main limitation of this analysis is that a potential role of charged clusters is not taken into account. Based on Eq. (1), a plot of the logarithm of the ratio positive/negative analyte ion yield versus the sum the gas-phase basicities $GB(M) + GB(M-H^-)$ of the matrices used should yield a straight line with a negative slope $(-1/RT)$ and an intercept that is related to the gas-phase basicities of the analyte. Unfortunately, only few of the necessary matrix GB values are known [20]. Nevertheless, we were able to obtain good numbers for DHB, 4NA, and ANP; the remaining values that were used are estimates.

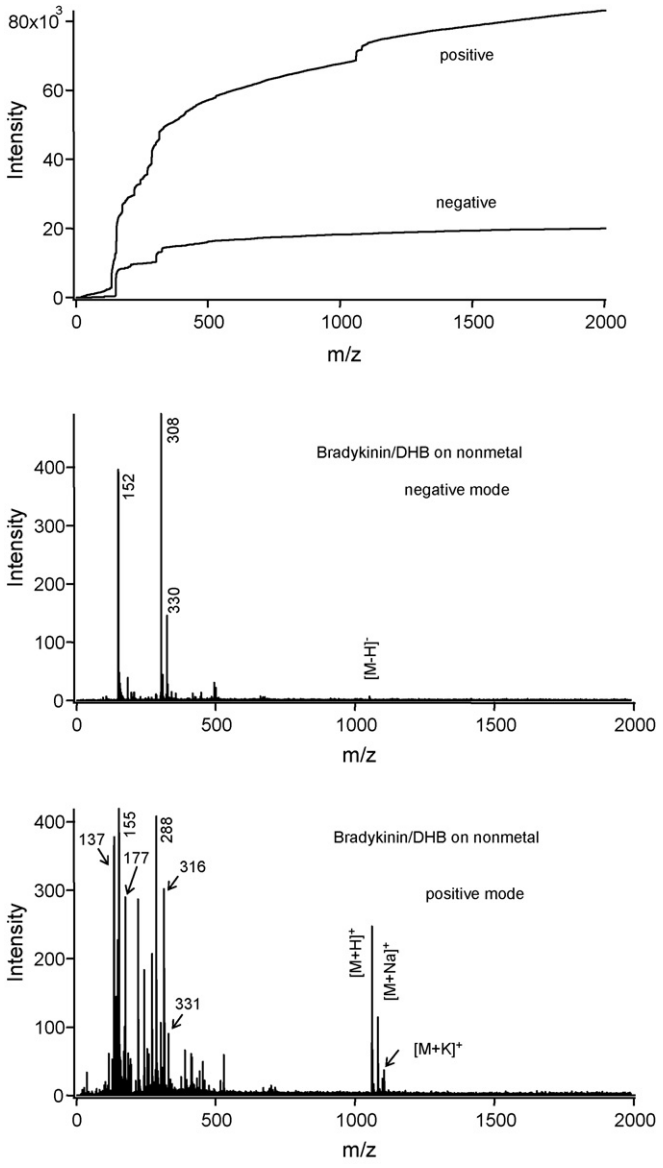

Fig. 3. Positive (bottom) and negative (middle) TOF mass spectra of bradykinin with DHB as a matrix on a stainless steel target covered with scotch tape, recorded on the AXIMA instrument. The integration of the spectra (top) corresponds to the total ion current. With the exception of polarity both spectra were taken under identical experimental conditions.

4. Results and discussions

Fig. 3 shows positive and negative mode mass spectra of bradykinin with DHB, recorded with the AXIMA instrument in Zürich. Both spectra were taken under typical identical experimental conditions and are not corrected for the detector bias, as discussed above. The integration of the mass spectra in both polarities, therefore, shows higher response for both analyte and total ion yields in positive mode. An interesting feature in this spectrum is that the integrals in both negative and positive mode rise steadily, even at *m/z* values well above the main peaks in the spectra. We interpret this to be due to "chemical noise", more precisely, to charged clusters and fragments of clusters that give rise to small peaks throughout the MALDI mass spectrum. This phenomenon is well known and has been very clearly described by Krutchinsky and Chait [21]. Fig. 4 shows positive and negative MALDI mass spectra of fibrinopeptide A, using CHCA as the matrix, recorded under identical conditions. Again some preference for positive ions is observed, as is a steady rise of the integrated signal intensity with mass. For comparison, some of these experiments were repeated on the FT-ICR instrument (data not shown). For example, FT-ICR spectra of bradykinin/DHB, prepared in exactly the same fashion as for the measurements on the AXIMA instrument, are very similar to the TOF data. The main difference when compared to the TOF data was that the total ion current, derived from the integral, was very close for the positive and negative polarity. Another important difference to the TOF data is that in FT-ICR, the much higher mass resolution leads to very narrow peaks and thus small peak integrals. On

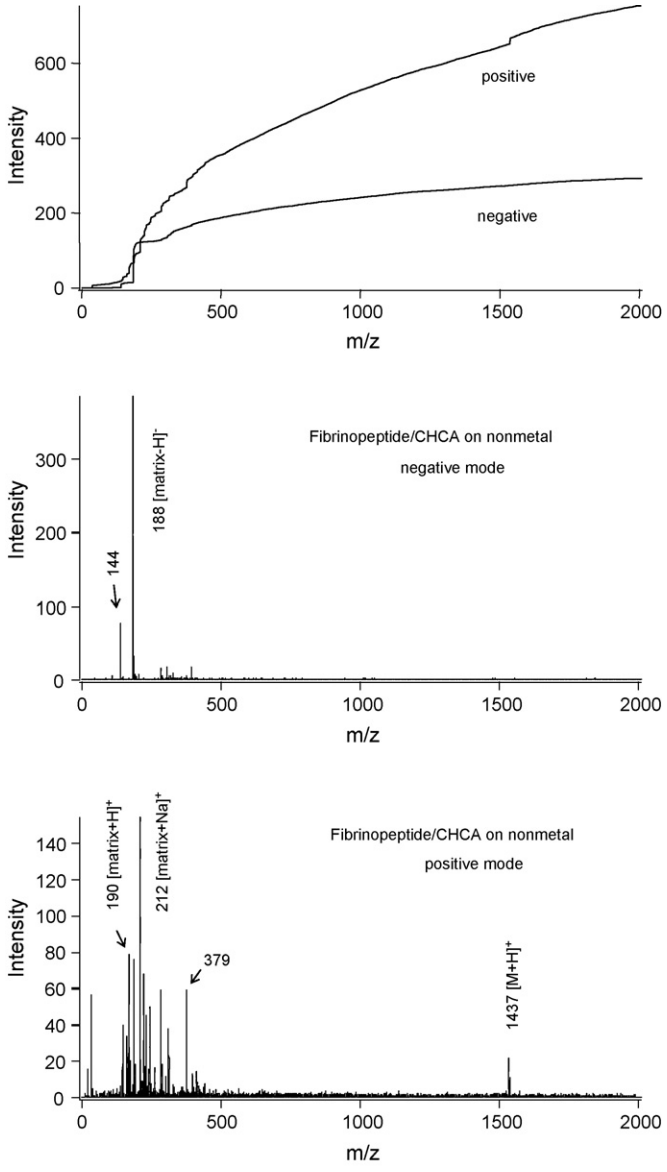

Fig. 4. Positive (bottom) and negative (middle) TOF mass spectra of fibrinopeptide A with CHCA as a matrix on a stainless steel target covered with scotch tape, recorded on the AXIMA instrument. The integration of the spectra (top) corresponds to the total ion current. With the exception of polarity both spectra were taken under identical experimental conditions.

the other hand, the chemical as well as electronic noise, which is integrated over the entire mass range, causes a much more pronounced increase of the integrated ion current with mass.

All experiments recorded on the AXIMA instrument were repeated several times, a standard deviation was calculated, and the data are summarized in Table 1 (numbers in italics). The values reported in this table are corrected by a factor of 3.5 that accounts for the larger detection efficiency for positive ions in the AXIMA instrument. MALDI spectra recorded with 5-AQ matrix showed only very weak random analyte signals for both bradykinin and fibrinopeptide on this instrument. The data is thus omitted from Table 1. The analyte positive/negative ion ratios covered a range between 0.5 (fibrinopeptide with ANP) and 3.7 (bradykinin with ANP); the error bars are large, due to large scatter in the data. This large scatter is, most probably, caused by the fact that the sample preparation was intentionally kept the same for all samples rather than being optimized for each analyte/matrix combination, to make intercomparison possibly. Also, sample spots were not selected for "sweet spots". The total ion yield, which is also reported in Table 1, was between 0.5 and 2.5 for all measurements, with an average of ≈1 when considering all measurements.

4.1. Measurements with charge detector

All results are summarized in Table 1. By far the best results were obtained for the DHB matrix, because ion signals were strong in both polarities and series of positive as well as negative ions could be recorded from the same sample spot. Sample spectra of angiotensin in both polarities, recorded with the SEM and charge detector are shown in Fig. 5. As expected, the positive ion spectra are dominated by the peptide signal at 1297 Da. No or only very small matrix signal were detected in this case, as is expected for the chosen analyte-to-matrix ratio of 10^{-3}. Negative ion spectra are dominated by the matrix signal at 153 Da but small peptide signals are also detected with both detectors. All four spectra were obtained from the same sample spot. Even though the spectra of the two polarities were always recorded from the same sample spot, the ratio of the signal intensities varied strongly from spot to spot, in the range of 0.33–6.04 for bradykinin, 1.1–4.25 for angiotensin and 0.39–1.78 for fibrinopeptide A. This observation is also corroborated by the fact that "sweet spots" of a given sample are not identical for positive and negative analyte ions. These numbers already point to the strong influence of the sample preparation on the relative ion yields. As was seen for the AXIMA instrument, the measured total ion signal ratio of positive to negative ion signals shows a large range of variation for all matrices, even though equal numbers of ions of either polarity should have been generated when desorbed from a dielectric substrate. The reason for this observation is, most probably, that a substantial fraction of the total charge is carried by clusters, mostly of matrix only, but some also containing analyte molecules. Such clusters extend to very high masses, i.e., milliseconds of flight time. Stable cluster ions would lead to a slow continuous increase of signal with mass which is hidden underneath the electronic signal decay induced by the time constant of the capacitive signal coupling unit. A certain fraction of these clusters undergoes metastable decay. As explained above, their PSD neutrals will diminish the signals of positive and enhance signals of negative ion spectra. Actually, the measured signal decay time constants showed values lower by typically 10–20% for positive ion spectra than those of negative ions, clearly indicating a contribution of metastable cluster decay. These differences are difficult to pick up by integration of spectra recorded with a MCP or a SEM, because they are the sum of very small signals over a long integration time (compared to the flight time of matrix and peptide ions), and the integral depends very critically on the exact position of the base line. No influence of metastable decay of matrix or peptide ions in the low mass range is visible in the spectra of Fig. 5. This was essentially true for most of the other matrices and analytes

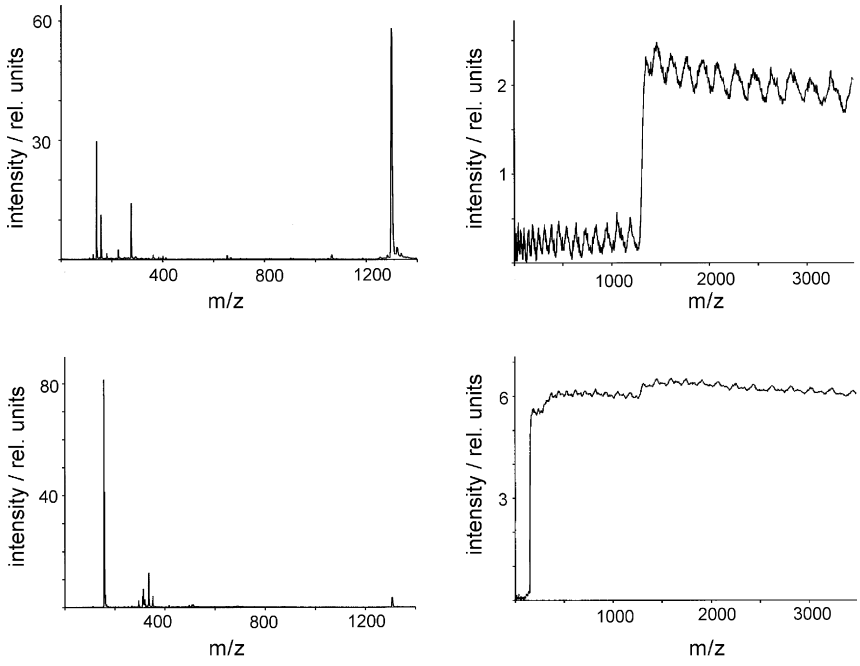

Fig. 5. Positive (top) and negative (bottom) sample spectra of a angiotensin/DHB sample. Molar analyte-to-matrix ratio 10^{-3}. Secondary electron multiplier spectra are shown on the right and charge detector spectra at the left. The intensity scales of the SEM and the charge detector, respectively, are intercomparable. All four spectra were recorded from the same sample spot.

as well, testifying that near threshold fluencies were used in all cases. Notable exceptions were fibrinopeptide A desorbed with CHCA and ATT as well as Bradykinin/5-AQ. At 1.5–2 times threshold fluence metastable decay of matrix and/or analyte ions was always clearly visible.

The values for the ratio of positive to negative ion signals for the other combinations of the three peptides and matrices show even more scatter, because spectra of the different polarities could never be recorded from identical sample spots, increasing the influence of the preparation and the well-known sweet spot phenomenon. For bradykinin and the matrices ATT and ANP the numbers should be considered only lower bounds, because clearly discernable negative ion signals could be obtained from only a very limited selection of sample spots much fewer than for positive ions.

Fig. 6 shows a plot for the three different analytes versus the six matrices, drawn in a semi-logarithmic fashion to test the validity of Eq. (1). Although some trend with a negative slope appears to be recognizable, the slope of the data is far too small to be compatible with Eq. (1) even if we assume an elevated temperature in the plume of several 100 K. Also, for fibrinopeptide A, an almost zero slope may be read from the plot, whereas the slope for bradykinin and angiotenin show no systematic trend or appear to be much greater. If Eq. (1) would accurately describe the situation, the slopes should be identical and larger for all analytes, and the only difference for different analytes should be in the intercept.

Our interpretation, therefore, is that effects other than gas-phase proton transfer in the plume dominate the outcome of the MALDI spectra [12,14,17,22]. One possibility is that other ion formation processes, such as the "lucky survivor" [17] or "exciton pooling" [15] pathways described in the literature are dominating. However, the expected ratio of positive/negative ions has yet to be predicted by these models. Other explanations for the disagreement of the data with the proton transfer theory invoke sample preparation (concentration, matrix-to-analyte ratio, microscopic morphology of the support, crystallization time), sample crystallinity, and sample homogeneity. For example, the size of matrix crystallites is expected to have an influence on the threshold laser fluence needed to cause efficient sample ablation. Also, it is now well established [21,23,24] that a large part of a MALDI sample is ablated in the form of clusters and

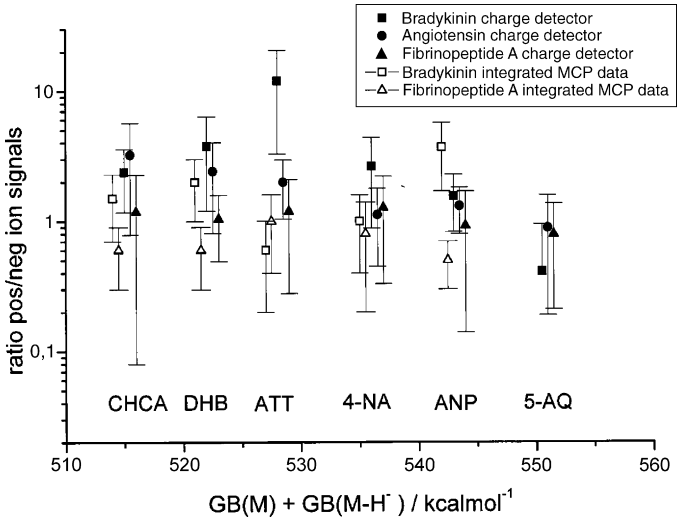

Fig. 6. Semi-logarithmic plot of $[(A+H)^-]/[(A-H)^-]$ vs. GB(M) + GB(M−H) of the matrix for three analytes and six different matrices. Solid symbols—charge detector data (Münster); open symbols—integrated microchannel plate data (Zürich).

chunks. In the context of determining the positive/negative ion yield ratio, the fraction of analyte that will appear in ionic form in the spectrum and contribute to the analyte ion yield in either polarity can be influenced by clusters. Analyte molecules "hidden" in the interior of larger clusters or chunks of material may never be observed as ions in the spectrum. The steady rise of the integrated ion signal in Figs. 3 and 4, and the observation of a contribution from PSD of higher molecular weight species clearly support the presence of large clusters.

The mean values of the ratio of positive-to negative analyte ion signals differ somewhat for the two instruments, but lie within each other's standard deviation, which is considered satisfactory, given the large scatter. The notable exception is the combination of bradykinine/ATT. Currently no explanation can be given for this result and the measurements will have to be repeated to determine whether this data point is simply an outlyer.

For some matrices, for example DHB and ANP, we did observe such a trend that follows the basicity of the analyte (Fig. 7). The plot itself does not imply any particular formation mechanism, but rather shows that with increasing basicity of the analyte, a larger positive/negative ion yield ration is found; this trend is more pronounced for the more acidic DHB matrix than for the basic ANP matrix. Attempts to plot the data for other matrices in the same fashion failed. While it is possible that the crystallinity of CHCA, ATT, 4-NA, and 5-AQ can be less well controlled and thus exercises a much greater influence on analyte ion formation than the gas-phase acid/base properties, the error bars on the data are currently too large to draw any firm conclusions about the dominant factor determining the positive/negative ion yield

One could argue that the molar ratio of analyte to matrix of 10^{-3} in the final preparation is too high for typical MALDI applications and the presented results, therefore, do not reflect standard MALDI conditions. While on the high side, it is not excessive for small mass peptides. Moreover, all samples have been looked at in the in TOFs with standard MCP or SEM detectors and the spectra look in no way different from ones obtained under more standard and optimized conditions, including, e.g., a strong matrix suppression for positive ion spectra and DHB.

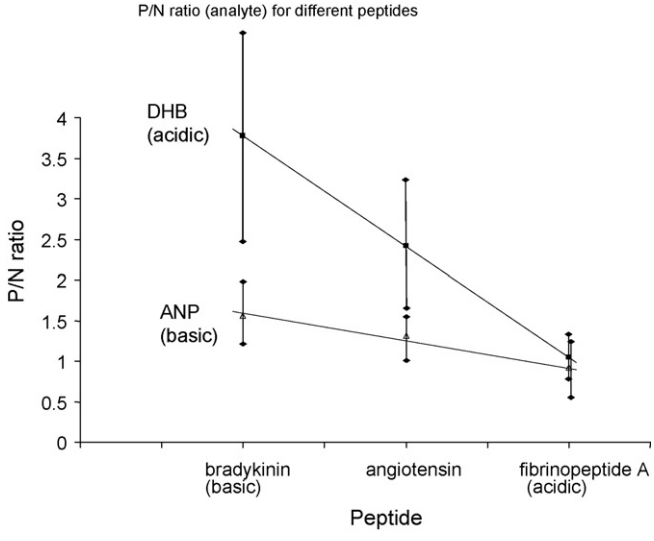

Fig. 7. Plot of the analyte positive/negative ion yield ratio vs. acid/base properties of the three peptides studied.

5. Conclusions

The dependence of the analyte ion yield on acid/base properties of the matrix and the analyte studied was examined. On average, the total ion yield in the negative mode approximately equaled that in the positive mode when MALDI samples were deposited on nonconductive substrates. However, we found an instrument-dependent detection bias, which for the commercial TOF instrument used in this study favored positive over negative ions by a factor of ≈3.5. On the instrument equipped with the charge detector, a slight excess of negative over positive (total) ions were found, probably a consequence of the different extent of PSD of higher molecular weight clusters in the positive and negative polarity. Very limited influence of PSD of matrix or peptide ions in the low mass range was discernible in the spectra.

When studying analyte ion yields, more acidic matrices were found to produce a positive/negative analyte ion yield ratio >1, whereas for basic matrices, the ratio was ≤1. However, an attempt to employ gas-phase protonation/deprotonation reactions for explaining the relative ion yields failed. While the large data scatter complicates the interpretation, the fact that not even the trend of the majority of the results follows the predicted dependence of the relative ion yields on matrix GB, speaks against gas phase proton transfer as the single or dominant ion formation process for analyte ions in MALDI. Although for selected matrices, the positive/negative analyte ion yield ratio nicely tracks the acid/base properties of the analyte, further experiments are necessary to test other models. Among them would be to determine the dependence of the ion yields on sample preparation. For selected matrices such as DHB, which generates strong ion signals in both polarities, one could cover a range of molar analyte-to-matrix ratios as well as the concentration of analyte and matrix in the dispensed sample. Both are expected to influence the crystallization and sample morphology. The same holds for different solvents which influence the drying speeds. Laser fluence as a significant contribution of clusters as carriers of the total charge in MALDI were obtained from the data. Clusters and cluster fragments cover a very large mass range and may be responsible for the overall low ion yield in MALDI.

References

[1] M. Karas, D. Bachmann, U. Bahr, F. Hillenkamp, Int. J. Mass Spectrom. Ion Process. 78 (1987) 53.
[2] M. Karas, D. Bachmann, F. Hillenkamp, Anal. Chem. 57 (1985) 2935.
[3] M. Karas, F. Hillenkamp, Anal. Chem. 60 (1988) 2299.
[4] I.A. Papayannopoulos, Mass Spectrom. Rev. 14 (1995) 49.
[5] K. Janek, H. Wenschuh, M. Bienert, E. Krause, Rapid Commun. Mass Spectrom. 15 (2001) 1593.
[6] S.-T. Tsai, C.W. Chen, L.C.L. Huang, M.-C. Huang, C.-H. Chen, Y.-S. Wang, Anal. Chem. 78 (2006) 7729.
[7] P.G. Carson, M.V. Johnston, A.S. Wexler, Rapid Commun. Mass Spectrom. 11 (1997) 993.
[8] C.D. Mowry, M.V. Johnston, J. Phys. Chem. 98 (1994) 1904.

[9] A.A. Puretzky, D.B. Geohegan, Chem. Phys. Lett. 286 (1998) 425.
[10] M. Dashtiev, V. Frankevich, R. Zenobi, J. Phys. Chem. A 110 (2006) 926.
[11] V.E. Frankevich, J. Zhang, S.D. Friess, M. Dashtiev, R. Zenobi, Anal. Chem. 75 (2003) 6063.
[12] R. Zenobi, R. Knochenmuss, Mass Spectrom. Rev. 17 (1998) 337.
[13] I. Fournier, A. Brunot, J.C. Tabet, G. Bolbach, Int. J. Mass Spectrom. 213 (2002) 203.
[14] M. Karas, R. Krüger, Chem. Rev. 103 (2003) 427.
[15] R. Knochenmuss, Anal. Chem. 75 (2003) 2199.
[16] R. Knochenmuss, J. Mass Spectrom. 37 (2002) 867.
[17] M. Karas, M. Glückmann, J. Schäfer, J. Mass Spectrom. 35 (2000) 1.
[18] H. Ehring, M. Karas, F. Hillenkamp, Org. Mass Spectrom. 27 (1992) 472.
[19] U. Bahr, U. Röhling, C. Lautz, K. Strupat, M. Schürenberg, F. Hillenkamp, Int. J. Mass Spectrom. Ion Process. 153 (1996) 9.
[20] K. Breuker, Proton transfer reactions in MALDI, Ph.D. Thesis Nr. 13351, ETH Zürich, Zürich, 1999.
[21] A.N. Krutchinsky, B.T. Chait, J. Am. Soc. Mass Spectrom. 13 (2002) 129.
[22] R. Knochenmuss, R. Zenobi, Chem. Rev. 103 (2003) 441.
[23] M. Handschuh, S. Nettesheim, R. Zenobi, Appl. Surf. Sci. 137 (1999) 125.
[24] L.V. Zhigilei, E. Leveugle, Chem. Rev. 103 (2003) 321.